Electronic Supplementary Information
There and back again: bridging meso- and nanoscales to understand lipid vesicle patterning

Julie Cornet[1], Nelly Coulonges[1,2], Weria Pezeshkian[3], Maël Penissat-Mahaut[2], Hermes Desgrez Dautet[4], Siewert J. Marrink[5], Nicolas Destainville[1], Matthieu Chavent[2,4], and Manoel Manghi[1]

(1) LPT, Université de Toulouse, CNRS, UPS, France
(2) Institut de Pharmacologie et Biologie Structurale, Université de Toulouse, CNRS, Université Toulouse III – Paul Sabatier, 31400, Toulouse, France
(3) Niels Bohr International Academy, Niels Bohr Institute, University of Copenhagen, Blegdamsvej 17, 2100 Copenhagen, Denmark
(4) Laboratoire de Microbiologie et Génétique Moléculaires (LMGM), Centre de Biologie Intégrative (CBI), Université de Toulouse, CNRS, UPS, France
(5) Groningen Biomolecular Sciences and Biotechnology Institute, University of Groningen, Nijenborgh 7, 9747 AG Groningen, The Netherlands

A. Cumulative effects of spontaneous curvature induced by insertions and by area difference

Spontaneous curvature can arise from either local molecular insertions with asymmetric shapes, such as lipids or proteins with global conical shapes, or from the difference of area between the two leaflets of the bilayer. This difference of areas comes from the history of the bilayer, the way its was created and equilibrated (or not). In this case, it is a non-local effect, at the origin of the Area Difference Energy (ADE) model [1, 2]. In Ref. [3], the cumulative effects of both curvatures is investigated. It is shown (see their Eq. (18)) that the resulting spontaneous curvature can be written as the weighted mean

$$C^* = \frac{\kappa K_\mathrm{B} + \kappa_{nl} K_s}{\kappa + \kappa_{nl}} \tag{S1}$$

where K_B and K_s are curvatures associated with asymmetric insertions and area difference, respectively, and κ and κ_{nl} are two bending moduli. It is argued in this work that $\kappa_{nl} \gg \kappa$ (a ratio of 6 is proposed) so that

$$C^* \simeq \frac{\kappa}{\kappa + \kappa_{nl}} K_\mathrm{B} + K_s \tag{S2}$$

When both leaflets have the same area, as in our planar geometry CG simulations, one has $K_s = 0$ so that the measured spontaneous curvature in presence of GM1 is $C^{\mathrm{planar}}_{\mathrm{Lo+GM1}} = \frac{\kappa}{\kappa+\kappa_{nl}} K_\mathrm{B}$. In vesicles where leaflet areas have had time to accommodate the spherical geometry, $K_s = 2/R$. We eventually get that when both effects are concomitantly at play, $C^* = C^{\mathrm{planar}}_{\mathrm{Lo+GM1}} + 2/R$. This C^* corresponds to our $C^{\mathrm{vesicle}}_{\mathrm{Lo+GM1}}$ in the main text. In other words, the curved species is endowed with a differential curvature $C^{\mathrm{planar}}_{\mathrm{Lo+GM1}}$ measured in planar geometry.

B. Estimate of bending moduli κ

We follow the strategy proposed by Ref. [4] to extract the bending modulus κ from a CG simulation of a tensionless bilayer made of a homogeneous lipid mixture. As made explicit in Eq. (12) of the main text, the membrane thermal shape fluctuations can be related to membrane parameters through Helfrich's model, to which a term accounting for protrusions has been added. To measure the Fourier mode amplitudes from CG simulation, we used the PO4 beads of phospholipids to identify both leaflets and used the Mathematica interpolation function (at order 1) to transform their positions into a continuous height function representing the membrane mid-surface, taking periodic boundary conditions into account, before Fourier-transforming it. Fitting with Eq. (12) of the main text, we got $\kappa_\mathrm{Ld} \simeq 13.1 \pm 0.3 k_\mathrm{B}T$ and $\kappa_\mathrm{Lo} \simeq 24 \pm 2 k_\mathrm{B}T$ (standard error are provided by the fitting procedure). We also found the value $\sigma_\mathrm{pr} \simeq 0.12$ J/m^2 for the tension associated with protrusions, in agreement with expectations. In Figure S1, we observe that the Lo data are more noisy than the Ld ones, even though both CG simulations were of equal duration. This might be due to the presence of GM1 bulky heads perturbing the bilayer order. For this reason, we round the measured value to $\kappa_\mathrm{Lo} = 25 k_\mathrm{B}T$ for the Lo phase. We also round the value to $\kappa_\mathrm{Ld} = 13 k_\mathrm{B}T$ for the Ld phase.

Now we compare these values to available experimental ones found in the literature. Indeed, many experimental techniques can also give access to the value of the bending modulus of a homogeneous phase, notably micropipette

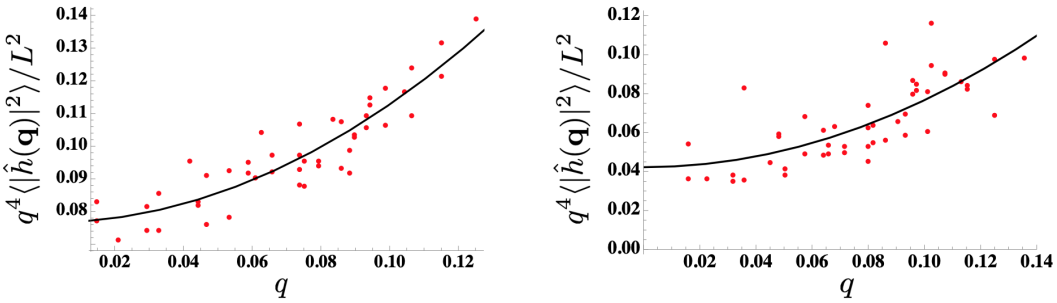

FIG. S1: Spectral densities (dots) from CG 10 μs simulations of $L \approx 40$ nm square patches. Ld (left) and Lo+GM1 (right) lipid mixture bilayers were simulated and the spectra fitted with Eq. (12) of the main text (black line), from which bending moduli are extracted. The wavevectors q are expressed in $\mathring{A}^{-1}$ and the vertical axis unit is $(k_BT)^{-1}$.

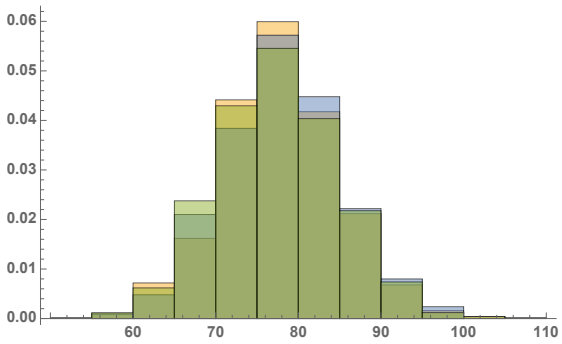

FIG. S2: Influence of the rigidity $\kappa_{\rm Ld}$ of the Ld phase on the nanodomain size distribution for $\kappa_{\rm Ld} = 6$ (green bars), 10 (blue) and $20k_BT$ (yellow). Nanodomain sizes are given in number of vertices in a given Lo-phase nanodomain in the Mesoscale model. The distribution is bimodal, however the monomer and small multimer peaks are not shown. Other parameter values are $\phi = 0.2$, $\kappa_{\rm Lo} = 20k_BT$, $C^{\rm vesicle}_{\rm Lo+GM1} = 5/R$, $J_I = 1/3.4 > J_{I,c}$, and $\tilde{\sigma} = 300$.

aspiration, measurements of vesicle shape fluctuations (flicker spectroscopy), NMR, electrodeformation, low angle diffuse X-ray scattering or neutron spin-echo. Note however that the so-obtained experimental values can appear to depend significantly on the experimental method used [5]. For a pure DPPC membrane explored by flicker spectroscopy just above the transition temperature, one measures a bending modulus on the order of $10k_BT$ [6]. The adjunction of 30% cholesterol increases this value by a factor ~ 2 at 44°C [7], as measured by NMR. This is consistent with the value $\kappa_{\rm Lo} \simeq 25k_BT$ found with our CG simulations, assuming that GM1 do not affect too much the Lo phase rigidity, being a minority species. For a pure DLiPC (DIPC in MARTINI) membrane, its bending rigidity has also been measured to be close to $10k_BT$ by micropipette aspiration at 18°C [8], also comparable to the value that we measured.

Finally, we checked that the exact choice of this latter value has no strong influence on the nanodomain statistics in the Mesoscale model because the Ld phase is assumed to have its spontaneous curvature set by the average vesicle radius and is only weakly curved. For example, in Fig. S2, we give the nanodomain size distributions for three different values of $\kappa_{\rm Ld}$ and see little influence of this parameter value.

C. Local thickness measurements

The local thickness can be calculated via the difference of position of the corresponding box centroids in the two leaflets, for the Ld and the Lo phase (Fig. S3). We find an average membrane thickness for all GM1 concentration of approximately 4 nm. As expected, the Lo phase is thicker than the Ld one. This explains why the Lo phase is more rigid than the Ld one. Indeed, in rough approximation, a membrane can be seen as an homogeneous elastic plate, the bending modulus of which grows as the cube of its thickness h:

$$\kappa = \frac{Eh^3}{12(1-\nu^2)} \tag{S3}$$

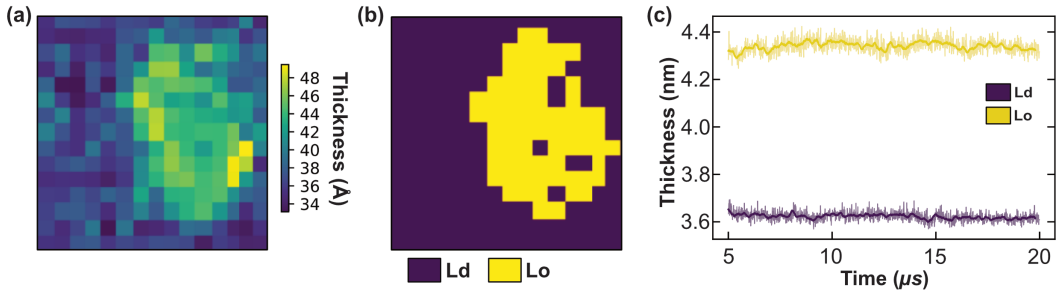

FIG. S3: **(a)** Local thickness h measured on the 15×15 mesh (in Å), compared to the binarized membrane **(b)**, for the same mixture as in Fig. 5 in the main text. **(c)** Local thickness (in nm) evolution with time after equilibration, measured separately for Lo and Ld phases. DPPC-DIPC-chol (30:58:12) mixture with no GM1. Here and in the following figures, the thick lines are sliding averages of the thinner ones on a 0.2 μs sliding window.

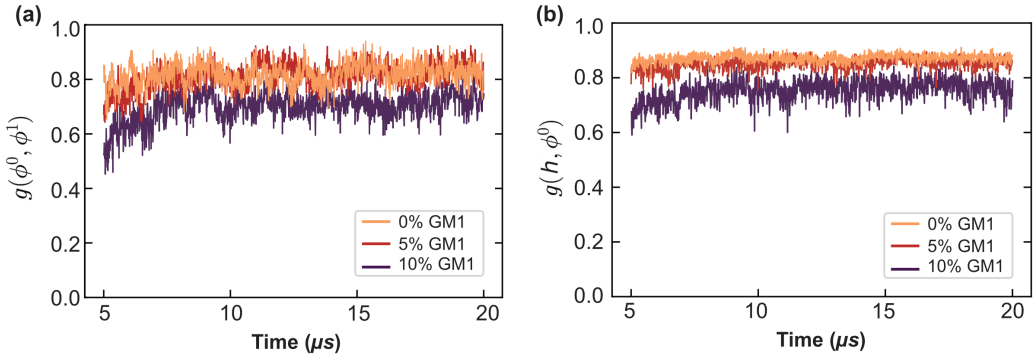

FIG. S4: **(a)** Correlation between the composition fields of the 2 leaflets (registration) through time. **(ab** Correlation between the composition field of the bilayer and the local thickness through time. DPPC-DIPC-chol (30:58:12) mixture with percentage of GM1 in the upper leaflet varying from 0 (orange), to 5 (red) and to 10 (purple).

assuming the same Young modulus E and Poisson ratio ν [9]. Using the average values shown in Fig. S3 (bottom), one finds $\kappa_{\rm Lo}/\kappa_{\rm Ld} \simeq (4.35/3.6)^3 \simeq 1.8$ in full agreement with our measures of $\kappa_{\rm Ld}$ and $\kappa_{\rm Lo}$.

D. Correlations

We measure the composition correlation between the two leaflets (registration) at a given time step following

$$g(\phi^0, \phi^1) = \frac{1}{N} \sum_{i,j} \frac{\phi^0_{ij}\phi^1_{ij} - \langle\phi^0\rangle\langle\phi^1\rangle}{s(\phi^0)s(\phi^1)} \tag{S4}$$

with ϕ^0 and ϕ^1 being the binarized compositions in the upper and lower leaflet respectively, and N the number of sites of the mesh taken into account (here $15^2 = 225$). We normalize it by the standard deviations s so to get a value ranging from -1 to 1. We check in Fig. S4 (left) that the leaflet compositions are indeed in register with $g(\phi^0, \phi^1) \simeq 0.8$.

Similarly, we compute the correlation between the local bilayer thickness h and the local composition ϕ of the bilayer (average box composition of both leaflets) defined as

$$g(h, \phi) = \frac{1}{N} \sum_{i,j} \frac{h_{ij}\phi_{ij} - \langle h\rangle\langle\phi\rangle}{s(h)s(\phi)} \tag{S5}$$

We notice in Fig. S4-b a strong correlation with $g(h, \phi) \simeq 0.9$, as expected.

We further compute $g(C, \phi^0)$ providing information about the correlation between the local curvature and the

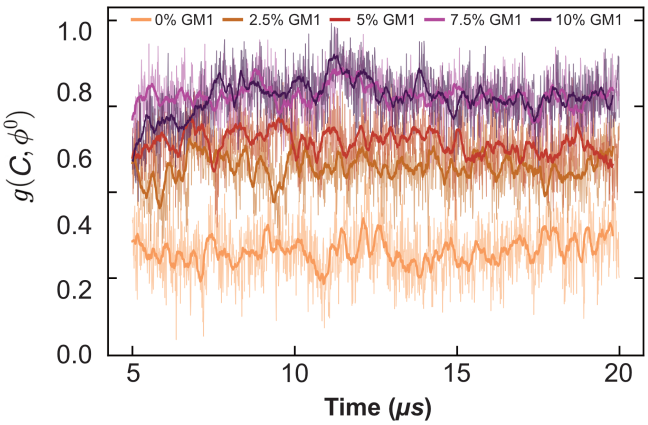

FIG. S5: Correlation between the composition field of the upper leaflet and the local curvature through time. DPPC-DIPC-chol (30:58:12) mixture with percentage of GM1 in the upper leaflet varying from 0 (orange) to 10 (purple) by steps of 2.5.

composition of the upper leaflet:

$$g(C,\phi^0) = \frac{1}{N}\sum_{i,j}\frac{C_{ij}\phi^0_{ij} - \langle C\rangle\langle\phi^0\rangle}{s(C)s(\phi^0)} \tag{S6}$$

with C being the local upper leaflet curvature. We measure in Fig. S5 a high correlation which appears to be higher in the Lo phase where GM1 are inserted. This correlation increases with GM1 fraction.

E. Using the relations between molecular and mesoscopic parameters

As an illustrative example, suppose that the Mesoscale simulations are run with an Ising parameter $J_I = 0.5k_BT$. The line tension measured for mixtures with 10% of GM1 is $\lambda \simeq 1.2$ pN, so that $a \simeq 5.6$ nm owing to Eq. (11) of the main text. One can then calculate the corresponding radius associated to the N-vertices vesicle simulated at the mesoscale, $R \simeq 75$ nm (for $N = 2562$, see Eq. (1)). For a measured local curvature of $C^{\rm planar}_{\rm Lo+GM1} \simeq 0.05$ nm^{-1} at 10% GM1 in the outer leaflet, one gets $RC^{\rm planar}_{\rm Lo+GM1} \simeq 3.8$ and thus $RC^{\rm vesicle}_{\rm Lo+GM1} \simeq 5.8$ as input value for the Lo-phase dimensionless spontaneous curvature in the Mesoscale simulations.

Conversely one could start from the value of the dimensionless $RC^{\rm vesicle}_{\rm Lo+GM1}$ used in Mesoscale simulations and infer the ensuing real-unit curvature $C^{\rm planar}_{\rm Lo+GM1}$ and thus the GM1 concentration required to have this value of $RC^{\rm vesicle}_{\rm Lo+GM1}$ in the Mesoscale model.

F. Relaxation times of boundary fluctuation modes

Relaxation times of the boundary fluctuations are defined as follows. We consider a quasi-circular domain of average radius R_0, the boundary of which fluctuates under thermal agitation. The wavelength associated with the Fourier mode n is $\Lambda_n = 2\pi R_0/n$. If the domain radius in polar coordinates is $r(\theta,t) = R_0[1 + u(\theta,t)]$, we denote by u_n the amplitude of mode n. It is a Gaussian random variable of zero mean [10]. Its auto-correlation function is defined as $C_n(s) = \langle u_n(t)u_n(t+s)\rangle$, averaged over realization or over a long trajectory. As discussed for example in Ref. [11], $C_n(s)$ decays exponentially with s, with a characteristic timescale τ_n, also denoted by $\tau(\Lambda_n)$, that we call the relaxation time of mode n in the present work.

Refs. [11] and [12] have discussed in detail the expected dependence of τ on n in the MD context. Hydrodynamic interactions play a key role because forces locally applied on the domain boundary by the line tension are propagated on the whole boundary by hydrodynamic flows. In the frame of the Saffman-Delbruck theory, a typical lengthscale plays an important role, the so-called Saffman-Delbruck length $L_{\rm SD} = h\eta_m/(2\eta_f)$. Here $L_{\rm SD}$, η_m and η_f are the viscosities of the membrane and the fluid, respectively, and h is the membrane thickness. In real lipid membranes $L_{\rm SD}$ falls typically between 100 nm and 10 μm. Depending on the ratio between $L_{\rm SD}$ and Λ_n, τ scales differently with Λ_n.

n	2	3	4
τ_n (μs)	0.67	0.175	0.125

TABLE I: Relaxation times of domain-boundary fluctuation modes for the MD simulations of the DPPC-DIPC-chol (30:58:12) mixture.

On lengh-scales $\Lambda_n \ll L_{\rm SD}$, 2D hydrodynamics inside the membrane dominates and the solvent friction can be neglected, so that

$$\tau_n \simeq \frac{4h\eta_m}{\lambda}\frac{R_0}{n} \propto \Lambda_n. \tag{S7}$$

where λ still denotes the line tension at the domain boundary. Note that in this case, if the viscosity of the Lo and Ld phases differ, it can be proven that the value of $h\eta_m$ entering Eq. (S7) is in fact the mean $h\eta_m = (h_{\rm Lo}\eta_{\rm Lo} + h_{\rm Ld}\eta_{\rm Ld})/2$ [11]. To our knowledge, the viscosity of DLiPC bilayers has not been measured experimentally so far. However, we reasonably assume that Ld phase is much less viscous than the Lo one, so that $h\eta_m \simeq h_{\rm Lo}\eta_{\rm Lo}/2$. Literature where viscosities of lipid mixtures are measured are relatively sparse. Owing to the latter relation, we can extract reliable values of $h\eta_m$ from experiments on lipid mixtures where the Lo phase is comparable to ours, at comparable temperature. In Ref. [13], a 1:2 DOPC (C18:1 dioleoyl PC)/DPPC + 30% Chol, i.e. 51:25:23 DPPC-DOPC-Chol is studied, with a Lo phase comparable to ours. A value of $h\eta_m \simeq 4\times10^{-10}$ Pa.m.s is found at about 305 K. We use this value in the main text. In addition, $\eta_{\rm f} = 0.69$ mPa.s for water at 310 K, hence $L_{\rm SD} \simeq 300$ nm, larger than the MD system size. Note that the measured values of membrane viscosities somewhat depends on the experimental technique, so this value is only indicative.

On lengh-scales $\Lambda_n \gg L_{\rm SD}$, 3D hydrodynamics in the surrounding solvent would dominate, and

$$\tau_n \simeq \frac{2\pi\eta_f}{\lambda}\frac{R_0^2}{n^2} \propto \Lambda^2. \tag{S8}$$

In the intermediate regime where Λ and $L_{\rm SD}$ are comparable, a more complex integral relation has also been derived [11].

To measure relaxation times in MD simulations, we use the same discretized dartboard as described in the main text Methods to get the discrete values of $u(\theta,t)$. We then make use of a combination of Fast Fourier Transform (FFT) and Wiener-Khintchine's theorem to compute $C_n(s)$, and we finally extract τ_n by fitting $\ln[C_n(s)]$ with an affine function.

In Table I, we give the relaxation times measured this way (in absence of GM1). The slowest mode is on the μs timescale for a 12 μs run (after 8 μs of equilibration), thus sampling of this mode is relatively poor and the uncertainty on τ_2 is expected to be relatively important. We nevertheless can fit the measured values with a power-law, and we find that $\tau \propto 1/n^{2.5} \propto \Lambda^{2.5}$. In spite of the uncertainties, this suggests that the system size is above the Saffman-Delbruck length $L_{\rm SD}$ where $\tau \propto \Lambda^2$, whereas we would have expected that $\Lambda \ll L_{\rm SD}$ with known experimental viscosities. This apparent discrepancy either comes from insufficient sampling or from a smaller CG bilayer viscosity. Indeed, it is known to be smaller than the real one by several orders of magnitude [14, 15], which significantly lowers the value of $L_{\rm SD}$ in CG simulations using the MARTINI force field. If timescales are to be directly extracted from simulations rather than experiments, one must take great care of this delicate issue.

G. Determination of transverse deformation modes timescales

Here we address the question of the transverse fluctuation timescale in the Mesoscale model. A well established theory [1, 16] provides the membrane friction constant per membrane unit area at wavevector $q = 2\pi/\Lambda$,

$$\zeta_\perp = 4\eta_{\rm f} q = \frac{8\pi\eta_{\rm f}}{\Lambda} \tag{S9}$$

We are again interested in vertex dynamics at the shortest wavelength $\Lambda = 2a$. Owing to Einstein's relation, the radial diffusion coefficient of an elementary membrane patch of area $A_0 = 4\pi R^2/N \sim a^2$ is thus $D_\perp = k_{\rm B}T/(\zeta_\perp A_0)$. In our Mesoscale simulations, radial MC moves are attempted with a spatial step $\delta r = \rho R$ (with $\rho = 0.007$ in most of our runs). Thus the physical timescale associated with (one-dimensional) radial MC moves is

$$\delta t_\perp = \frac{\delta r^2}{2D_\perp} = \frac{2\pi\eta_{\rm f}\delta r^2 A_0}{k_{\rm B}Ta} \tag{S10}$$

If $R = 30$ nm and $N = 2562$, we obtain $\delta t_\perp = 90$ ps. Compared to the time-scale δt associated with vertex-composition flips above, it is much shorter (see main text).

H. Backmapping from the Mesoscale model to the CG one

In complement of Fig. 12 in the main text, Fig. S6 illustrates that the fraction of Lo triangles remains stable during the CG-MD simulation, very close to the initial 20% fraction before backmapping.

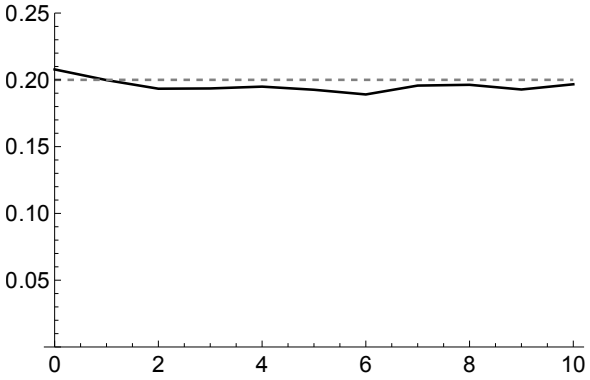

FIG. S6: Evolution with time of the fraction of Lo triangles (full line) and expected value of 20% (dashed line).

In addition, we measured the acyl-chain order parameter [17]

$$P = \frac{1}{2}\left(3\langle\cos^2(\theta)\rangle - 1\right) \tag{S11}$$

where θ is the angle between bond vectors between the lipid CG beads and the local bilayer normal (Figure S7-c, inset). It is commonly used to characterize chain ordering in the different lipid phases.

Due to the curvature induced by the GM1 lipids, we needed to modify the conventional way of measuring order parameters by considering the true local vector orthogonal to the membrane surface, rather than solely relying on the z vector commonly used as an approximation for the membrane normal vector. While this approximation holds true for simulations of almost planar membrane such as the beginning of our simulation (see Figure S7-a), it becomes inadequate towards the end of the simulation (see Figure S7-b). In brief, our script segments the membrane system into patches, calculates the local normal of each membrane patch, and computes the average order parameter for each lipid bond with respect to this local normal vector. On the vesicle (see Figure S7-e), the patches have variable sizes because of the inherent difficulty to divide a sphere in equal patches. This analysis specifically focuses on the upper leaflet, where GM1 is incorporated.

As expected, the order parameter of unsaturated DIPC lipids, concentrated in the Ld phase, rapidly drops for the extremities of the lipid located deeper into the bilayer, while saturated DPPC lipids, concentrated in the Lo phase, display acyl chain extremities more ordered in the bilayer core with an higher order parameter. Notably, the order parameter for DPPC exhibits a slight initial increase during the first 5 µs of simulations in the planar system (Figures S7-c and d), indicating a transient equilibration phase, while it remains relatively stable in the case of the vesicle (Figures S7-f and g), as this lipid is consistently maintained in a liquid-ordered phase. The order parameter values are not significantly different in the planar and vesicular systems. Further analyses will be necessary to further elaborate on these findings, especially by varying the temperature to observe the evolution of the order parameter, as previously conducted [17].

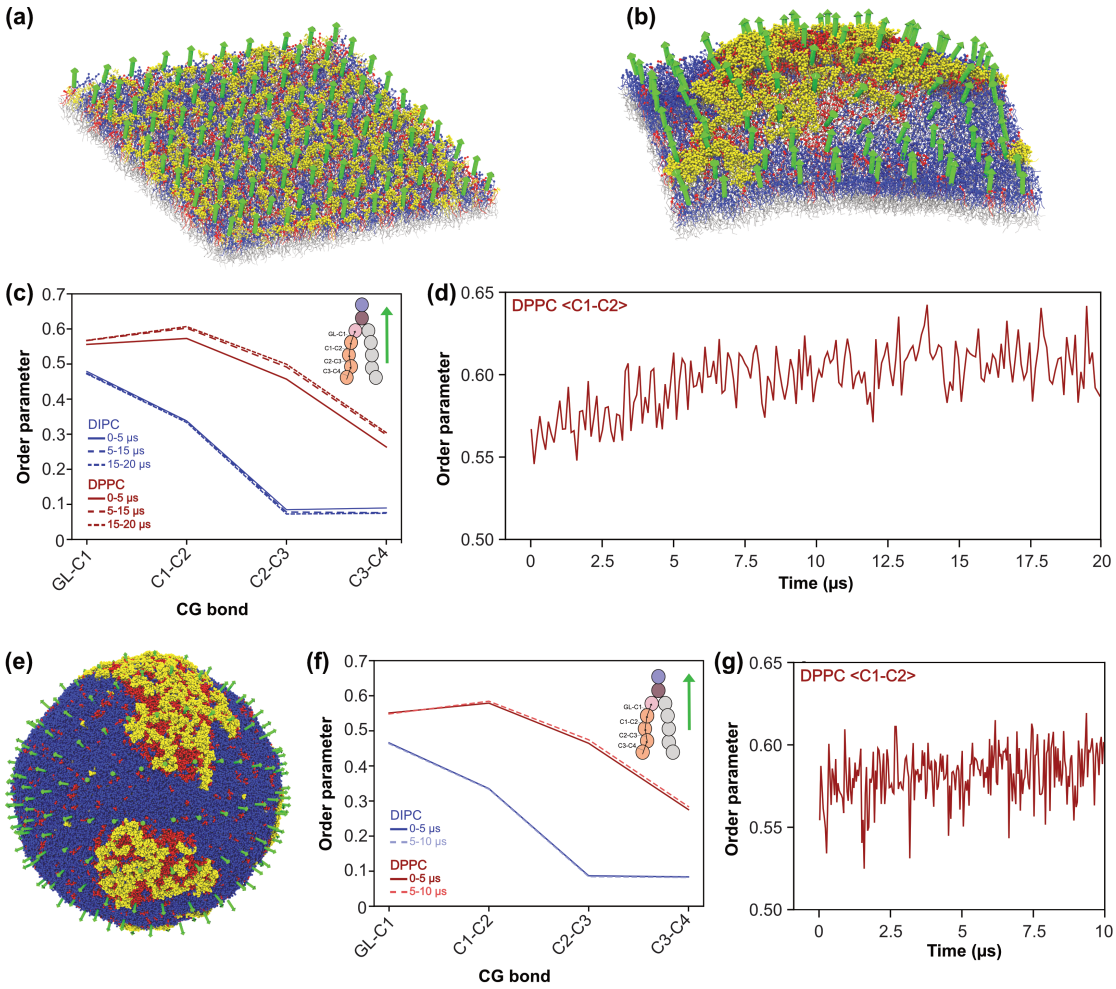

FIG. S7: Acyl chain order parameter P of 15% GM1 systems. **(a, b)** Visualization of the normal vectors (in green) to the 15% GM1 bilayer **(a)** at t=0 and **(b)** at t=20 μs used to calculate the order parameter for curved membranes. **(c)** Order parameter for DPPC and DIPC lipids extracted from the 15% GM1 planar system (upper leaflet). Inset: the different bonds, the orientation of which is measured with respect to the normal vector, in green. **(d)** Order parameter for DPPC C1-C2 bond during the course of the 20 μs simulation. **(e)** Vesicle system containing 15% of GM1 after backmapping from the mesoscale model and the normal vectors in green. **(f)** Order parameter for DPPC and DIPC lipids extracted from the 15% GM1 vesicle system. **(g)** Order parameter for DPPC C1-C2 bond during the course of the 10 μs simulation.

[1] U. Seifert, Advances in Physics **46**, 13 (1997).
[2] O. Mouritsen, Chemistry and Physics of Lipids **135**, 105 (2005).
[3] A. Hossein and M. Deserno, Biophysical Journal **118**, 624 (2020).
[4] P. W. Fowler, J. Hélie, A. Duncan, M. Chavent, H. Koldsø, and M. S. P. Sansom, Soft Matter **12**, 7792 (2016).
[5] M. Doktorova, D. Harries, and G. Khelashvili, Phys. Chem. Chem. Phys. **19**, 16806 (2017).
[6] L. Fernandez-Puente, I. Bivas, M. D. Mitov, and P. Méléard, Europhysics Letters (EPL) **28**, 181 (1994).
[7] G. Orädd, V. Shahedi, and G. Lindblom, Biochimica et Biophysica Acta (BBA) - Biomembranes **1788**, 1762 (2009).
[8] W. Rawicz, K. Olbrich, T. McIntosh, D. Needham, and E. Evans, Biophysical Journal **79**, 328 (2000).
[9] L. Landau, E. Lifshitz, A. Kosevich, J. Sykes, L. Pitaevskii, and W. Reid, Theory of Elasticity: Volume 7, Course of theoretical physics (Elsevier Science, 1986), ISBN 9780750626330.
[10] C. Esposito, A. Tian, S. Melamed, C. Johnson, S.-Y. Tee, and T. Baumgart, Biophysical Journal **93**, 3169 (2007).
[11] B. Camley, C. Esposito, T. Baumgart, and F. Brown, Biophysical Journal **99**, L44 (2010).
[12] B. Camley and F. Brown, Physical Review Letters **105**, 148102 (2010).
[13] E. Petrov and P. Schwille, Biophysical Journal **94**, L41 (2008).

[14] W. den Otter and S. Shkulipa, Biophysical Journal **93**, 423 (2007).
[15] M. Vögele, J. Köfinger, and G. Hummer, The Journal of Physical Chemistry B **123**, 5099–5106 (2019).
[16] U. Seifert and S. Langer, Europhysiccs Letters **23**, 71 (1993).
[17] Y. Liu, J. Barnoud, and S. J. Marrink, Biophysical Journal **117**, 1215 (2019).